Biosensors and Bioelectronics 89 (2017) 525–531

Contents lists available at ScienceDirect

Biosensors and Bioelectronics

journal homepage: www.elsevier.com/locate/bios

Surface Plasmon Resonance based sensing of lysozyme in serum on *Micrococcus lysodeikticus*-modified graphene oxide surfaces

Alina Vasilescu [a,*], Szilveszter Gáspár [a], Mihaela Gheorghiu [a], Sorin David [a], Valentina Dinca [b], Serban Peteu [c], Qian Wang [d,e], Musen Li [e], Rabah Boukherroub [d], Sabine Szunerits [d,**]

[a] International Center of Biodynamics, 1B Intrarea Portocalelor, Sector 6, 060101 Bucharest, Romania
[b] National Institute for Laser, Plasma and Radiation Physics (INFLPR), Str Atomistilor 409, PO Box MG-36, 077125 Magurele, Bucharest, Romania
[c] Department of Chemical Engineering and Materials Science, Michigan State University, 428 s Shaw Lane, East Lansing, Michigan 48824-1226, United States
[d] Institute of Electronics, Microelectronics and Nanotechnology (IEMN), UMR CNRS 8520, Lille1 University, Avenue Poincaré-BP60069, 59652 Villeneuve d'Ascq, France
[e] Key Laboratory for Liquid-Solid Structural Evolution and Processing of Materials (Ministry of Education), Shandong University, Jinan 250061, China

ARTICLE INFO

Article history:
Received 9 December 2015
Received in revised form
22 February 2016
Accepted 17 March 2016
Available online 19 March 2016

Keywords:
Graphene oxide
Layer-by-layer
Whole cell biosensor
Lysozyme
Surface Plasmon Resonance
Serum

ABSTRACT

Lysozyme is an enzyme found in biological fluids, which is upregulated in leukemia, renal diseases as well as in a number of inflammatory gastrointestinal diseases. We present here the development of a novel lysozyme sensing concept based on the use of *Micrococcus lysodeikticus* whole cells adsorbed on graphene oxide (GO)-coated Surface Plasmon Resonance (SPR) interfaces. *M. lysodeikticus* is a typical enzymatic substrate for lysozyme. Unlike previously reported sensors which are based on the detection of lysozyme through bioaffinity interactions, the bioactivity of lysozyme will be used here for sensing purposes. Upon exposure to lysozyme containing serum, the integrity of the bacterial cell wall is affected and the cells detach from the GO based interfaces, causing a characteristic decrease in the SPR signal. This allows sensing the presence of clinically relevant concentrations of lysozyme in undiluted serum samples.

1. Introduction

Lysozyme, a protein found in biological fluids such as tears, saliva, serum or urine is often called "body's own antibiotic". This name is related to its enzymatic activity as lysozyme hydrolyses the glycosidic bonds between N-acetyl muramic acid and N-acetyl glucose amine in peptidoglycans present in the cellular wall of Gram-positive bacteria. A typical protocol for determining its enzymatic activity relies on the use of a suspension of *Micrococcus lysodeikticus* cells. The turbidity of the suspension changes upon addition of lysozyme and is monitored through a change in optical absorbance at 450 nm (Avanti et al., 2014). As increased human lysozyme concentrations in serum and urine were associated with leukemia, renal diseases, as well as several gastrointestinal inflammatory conditions (Prockop and Davidson, 1964, Osserman and Lawlor, 1966, Perillie et al., 1968, Rubio, 2014), the development of fast and easy means of detecting lysozyme in different media became crucial. Only a few reports show, however, the sensitivity and selectivity required for sensing in real biological samples, achieved using different signal amplification strategies (Cheng et al., 2007, Hun et al., 2010, Li et al., 2010, Ocana et al., 2015).

The SPR based sensing of lysozyme, relying on the binding to surface-linked receptors such as aptamers or molecularly imprinted polymers was shown to be highly promising for the sensing of lysozyme (Matsunaga et al., 2007, Sener et al., 2011, Wang et al., 2011, Subramanian et al., 2013, Mihai et al., 2015). An approach for achieving the sensitivities required for the detection of lysozyme in serum is the use of SPR interfaces coated with graphene-related materials (Subramanian et al., 2013). Different dielectric coated plasmonic interfaces have shown their potential for highly sensitive sensing of analyte-ligand interactions (Abdulhalim et al., 2008, Szunerits et al., 2008, Touahir et al., 2010, Shalabney and Abdulhalim, 2011, Szunerits et al., 2012). In contrast to these multilayered SPR interfaces, the excellent sensing properties of graphene-coated SPR chips are related to the spontaneous adsorption of hydrophobic domains and π-electron rich systems present in biomolecules on graphene-based interfaces, and their electrostatic interactions with oxygen functional groups present on graphene oxide (GO) and reduced graphene oxide (rGO)

* Corresponding author.
** Corresponding author.
E-mail addresses: avasilescu@biodyn.ro (A. Vasilescu), sabine.szunerits@univ-lille1.fr (S. Szunerits).

http://dx.doi.org/10.1016/j.bios.2016.03.040
0956-5663/

(Subramanian et al., 2013, Szunerits et al., 2013, Zagorodko et al., 2014, Singh et al., 2015, Zagorodko et al., 2015). While monolayers of graphene on SPR interfaces have been used by some of us (Szunerits et al., 2013, Zagorodko et al., 2014, Zagorodko et al., 2015) and more recently by Cosnier and co-workers (Singh et al., 2015) for the construction of sensitive DNA, protein and immunosensors, the use of GO coated interfaces is a viable alternative (Zhang et al., 2013a, 2013a, 2013b). In particular, we have shown that electrophoretically deposited rGO, when modified with aptamers, allows for the sensitive and selective detection of lysozyme with a detection limit of 0.5 nM (Subramanian et al., 2013).

Among the approaches used for coating GO onto gold, direct deposition became an interesting and simple alternative, achievable *via* the interaction between a positively charged gold interface and the negatively charged GO (Mao et al., 2011, Wang et al., 2011, Huang et al., 2013, Ma et al., 2013, Chung et al., 2015). The layer-by-layer (LBL) approach, based on the successive deposition of compounds with opposite charges is advantageous for developing graphene-based biosensors as it allows obtaining multilayer coatings with controlled composition, thickness and functionality (Ma et al., 2013). For example, a composite, based on cationic polyelectrolyte-functionalized ionic liquid decorated graphene sheets, was synthesized and included in a multilayer film with Prussian blue *via* LBL assembly (Mao et al., 2011). This method allowed the detection of hydrogen peroxide by monitoring both SPR optical signals and electrochemical current responses. Label-free, regenerable, and sensitive SPR electrochemical aptasensors based on graphene were reported for the detection of α-thrombin (Wang et al., 2011). The deposition of GO bilayers on plasmonic substrates *via* LBL self-assembly and biomolecular sensing using BSA and anti-BSA antibody was recently demonstrated (Chung et al., 2015). While increased adsorption of proteins such as BSA (Chiu and Huang, 2014) or lysozyme (Li et al., 2014) on GO holds promise for biosensing or selective separation from complex mixtures, adsorption of whole bacterial cells on GO or rGO was less exploited (Subramanian et al., 2014).

In the present work, we investigate whether the presence of *M. lysodeikticus* on GO-modified sensing interfaces would allow for a selective detection of lysozyme in serum. For this, SPR interfaces were modified with GO *via* LBL assembly based on the strong electrostatic interaction between polycationic poly(diallyldimethylamonium) (PDDA) and negatively charged GO. *M. lysodeikticus* is then immobilized onto the GO-coated SPR interfaces. The interaction between serum samples spiked with lysozyme and GO thin films modified with *M. lysodeikticus* was followed in real time by SPR.

2. Materials and methods

2.1. Materials

Hydrogen peroxide was purchased from Carl Roth GmbH (Germany) and potassium hexacyanoferrate (III) from Merck (Germany). Human IgG was purchased from Fluka (Germany). Fetal bovine serum (FBS), bovine serum albumin (BSA), trypsin and penicillin/streptomycin were provided by Gibco. Graphene oxide, hen-egg lysozyme, *M. lysodeikticus*, poly(diallyldimethylamonium) (PDDA) and all other reagents were from Sigma-Aldrich, Germany.

2.2. Fabrication of Micrococcus lysodeikticus modified SPR interfaces

Gold SPR chips were immersed alternatively into aqueous solutions of PDDA (5%) in 0.1 M NaCl and GO (0.1 mg/mL) for 15 min each time. Between switching to the next solution, the interfaces were rinsed with water and dried under a nitrogen stream. The PDDA/GO modified SPR interfaces were furthermore modified with *M. lysodeikticus* by dropping 100 μL of 1 mg/mL bacterium solution onto the interface and then allowed to stand overnight at 2–8 °C in humidity-saturated atmosphere. The modified interfaces were rinsed with water, dried under nitrogen stream and kept at 2–8 °C until use. Further incubation in BSA (3%) solutions for 1 h provided non-fouling interfaces for sensing in serum.

2.3. Instrumentation

Electrochemical measurements were performed using a VSP potentiostat/galvanostat (from Bio-Logic S.A., France), equipped with the EC-Lab software, in a conventional 3-electrode setup that includes a SPR gold interface as working electrode, a Ag/AgCl (3 M) reference electrode, and a Pt counter electrode. Cyclic voltammetry experiments were performed in 5 mM potassium ferricyanide/ferrocyanide solution in 0.1 M KCl while the potential was scanned between −0.3 and +0.6 V *vs*. Ag/AgCl, 3 M KCl at 0.1 V/s.

SPR studies were performed using a SPREETA system (Nomadics Inc., USA) connected to a syringe pump and a computer for data acquisition and processing. A 2-channel polydimethylsiloxane (PDMS, Sylgard 184, Dow Corning, USA) flow cell was fitted to the SPR system. The system was controlled by a Labview-based software, developed at the International Centre of Biodynamics, Bucharest (ICB). The Au interfaces used for SPR testing were formed using physical vapour deposition and consist in a 50 nm Au layer deposited on glass with a 3 nm Ti adhesion layer. Prior to modification with PDDA and GO the interfaces were cleaned by overnight immersion in a 1:10 hypochlorite aqueous solution, followed by 10 min in a 1:1 0.5 M KOH: 30% H_2O_2 mixture. Between these steps and at the end of cleaning, the gold chips were washed with Millipore water and then dried under a stream of nitrogen.

Complementary SPR assays were done using an Autolab ESPRIT SPR instrument (Eco Chemie, The Netherlands) (Subramanian et al., 2014). The prism used was N-BAF-3 having a refractive index of $n=1.58$. WinSpall 2.0 software (Max-Planck-Institute for Polymer Research, Mainz) was used to calculate the SPR curves and approximate the experimental dependencies with an optical model within the framework of Maxwell macroscopic approach.

Atomic Force Microscopy (AFM) images were obtained using a Nanowizard II instrument (from JPK Instruments AG, Germany), silicon PPP-NCSTPt cantilevers (resonance frequency 76–263 kHz, force constant 1.2–29 N/m, from Nanosensors, Switzerland) and intermittent contact mode in air (setpoint ~690 mV, line rate 0.3 Hz). The lines of the AFM images were corrected by matching height median using Gwyddion software (version 2.26).

Static contact angles (CA) were measured with a CAM 100 goniometer (KSV Instruments, Finland) and water as the test liquid. CA values were generated using the CAM 100 software. The accuracy was ±2°. All measurements were made in ambient atmosphere at room temperature.

Scanning electron microscopy (SEM) images of the films were obtained using FEI Nova NanoSEM 450 scanning electron microscope with FEG (field emission gun, Schottky type) systems equipped with an energy dispersive X-ray analyzer at an accelerating voltage of 20 kV.

Micro-Raman spectroscopy measurements were performed on a Horiba Jobin Yvon LabRam HR Micro-Raman system combined with a 473-nm laser diode as excitation source. Visible light was focused by a 100× objective to the interface.

3. Results and discussion

3.1. Formation of Micrococcus lysodeikticus modified plasmonic interfaces

While the transfer of CVD graphene onto gold has the

advantage of using high quality graphene and offers control over the number of graphene layers, the strategy implies that one has access to CVD grown graphene (Szunerits et al., 2013, Zagorodko et al., 2014, Singh et al., 2015, Zagorodko et al., 2015). The direct deposition of GO onto gold is an appealing alternative achieved through the interaction between a positively charged gold interface and the negatively charged GO (Mao et al., 2011, Wang et al., 2011, Huang et al., 2013, Chung et al., 2015). As shown in Fig. 1, a LBL approach, using subsequently positively charged PDDA and negatively charged GO, was employed to build up PDDA- and GO-modified SPR interfaces. SEM was used to characterise the surface morphology of gold before and after modification with two layers of PDDA/GO (Fig. 2**A**). The raised bright strips clearly indicate the formation of smooth GO coated gold interfaces as previously reported (Huang et al., 2013). Fig. 2**B** shows the Raman spectra of GO and that of the SPR chip coated with PDDA/GO (two layers). The spectra display the main features of graphene-based materials with a D-band at 1351 cm^{-1} and a G-band at 1595 cm^{-1} with a 0.71 D-to-G intensity ratio for GO and $I_D/I_G = 1.01$ for GO deposited on gold-PDDA interfaces. The smaller I_D/I_G peak intensity ratio for GO corresponds to lower density of defects/disorder in the graphitized structure. The presence of GO was in addition validated by contact angle measurements, where the water contact angle of gold ($76 \pm 2°$) changed to $27 \pm 2°$ after PDDA deposition, and to $36 \pm 2°$ after GO addition.

The SPR spectra of the Au, Au-PDDA and Au-$(PDDA/GO)_n$ (1^{st}, 2^{nd} and 3^{rd} sequential immersions into PDDA and GO) modified interface are seen in Fig. 2**C**. The angle resolved SPR curves show that the addition of PDDA has no significant effect on the shape of the SPR curve, while further addition of GO results in an increase in the SPR angle, indicating the spontaneous electrostatic assembly of GO on PDDA (Wang et al., 2011). Curve fitting of the Au-$(PDDA/GO)_1$ suggests that the thickness of the transferred GO layer is ≈ 1.3 nm.

Sequential immersion into PDDA and GO for a second and third time shifts the SPR signal further to higher angles, as expected, concomitant with a broadening of the dip. An additional ≈ 1.3 nm thick layer is transferred in both cases confirming the uniformity of the layer-by-layer process. The reproducibility of the formation of Au-$(PDDA/GO)_2$ coated sensors was evaluated based on the measurement of angle-resolved SPR curves. An RSD of 9.3% was calculated for n = 5 coated sensors produced in the same batch. We opted in the following for working with Au-$(PDDA/GO)_2$, as it proved to be the best compromise between an increased immobilization capacity for biomolecules, associated with a higher GO content and an adequate sensitivity for SPR detection. Functionalization with *M. lysodeikticus* cells was achieved by overnight incubation of Au-PDDA/GO sensors with solutions containing 1 mg/mL bacteria. Upon modification of the sensors with bacterial cells the water contact angle decreased to $12 \pm 2°$ (n = 3 sensors).

All the steps in biosensor fabrication and the detection principle were also verified by cyclic voltammetry using $[Fe(CN)_6]^{4-/3-}$ as redox probe. The gold SPR interface gave voltammograms with a peak separation of $\Delta E_p = 0.19 \pm 0.03$ V, and a ratio between the current intensity of anodic and cathodic peaks of 1.01 ± 0.03, indicating a quasi-reversible electrochemical response. Upon coating with 2 layers of PDDA/GO, ΔE_p increases to 0.23 ± 0.04 V and the intensity of anodic and cathodic peaks diminishes (Fig. S1). Further modification by adsorption of *M. lysodeikticus* results in even smaller anodic and cathodic peaks and increased separation of ΔE_p (Fig. S1). Depending on the incubation time, cyclic voltammetry allowed to follow the density of the bacterial cells on the PDDA/GO interface. A progressive decrease in the intensity of anodic and cathodic peaks is observed upon longer incubation times (Fig. S1). To ensure maximum sensitivity and reproducibility of the sensor interface for an accurate quantification of lysozyme, the surface concentration of the bacterial substrate should be at the saturation level. To ensure adsorption of maximum quantities of bacteria, the PDDA/GO sensors were incubated overnight with *M. lysodeikticus*.

The morphology of the immobilized cells was determined by AFM in intermittent contact mode. Fig. 3 demonstrates that *M. lysodeikticus*, with a diameter of ≈ 1.1 μm and height of ≈ 0.58 μm arrange in irregular clusters on the Au-$(PDDA/GO)_2$ interface. The ability of the newly developed whole cell biosensor thus obtained to detect lysozyme in serum was investigated next by SPR.

3.2. SPR based detection of lysozyme in serum

The SPR setup used for the analysis of lysozyme in serum is based on two flow-through channels. One channel was used to

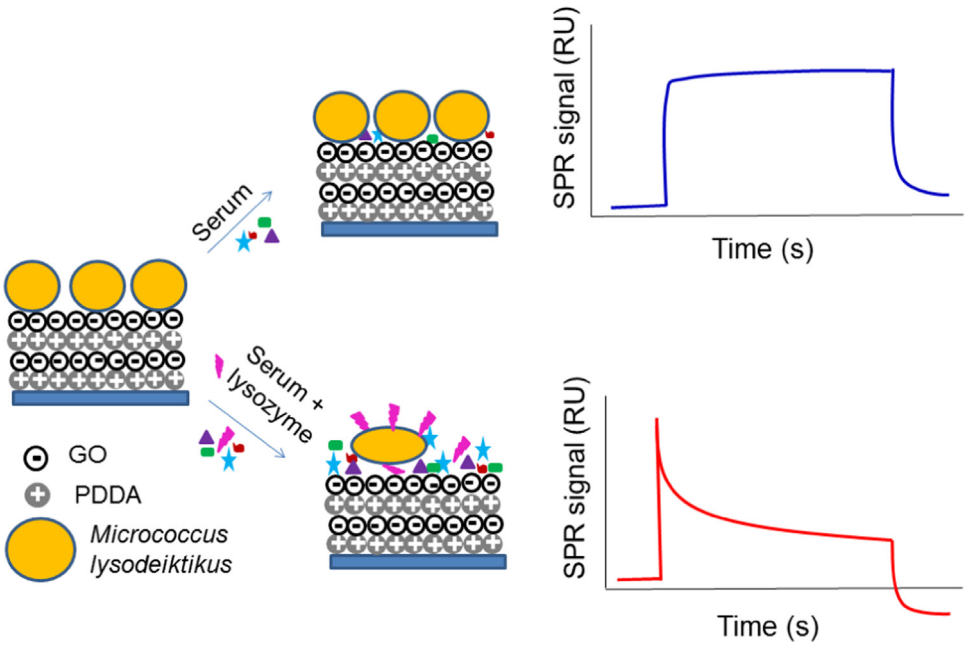

Fig. 1. Schematic representation of the sensing interface and the detection of lysozyme in serum based on the detection of lysozyme bioactivity.

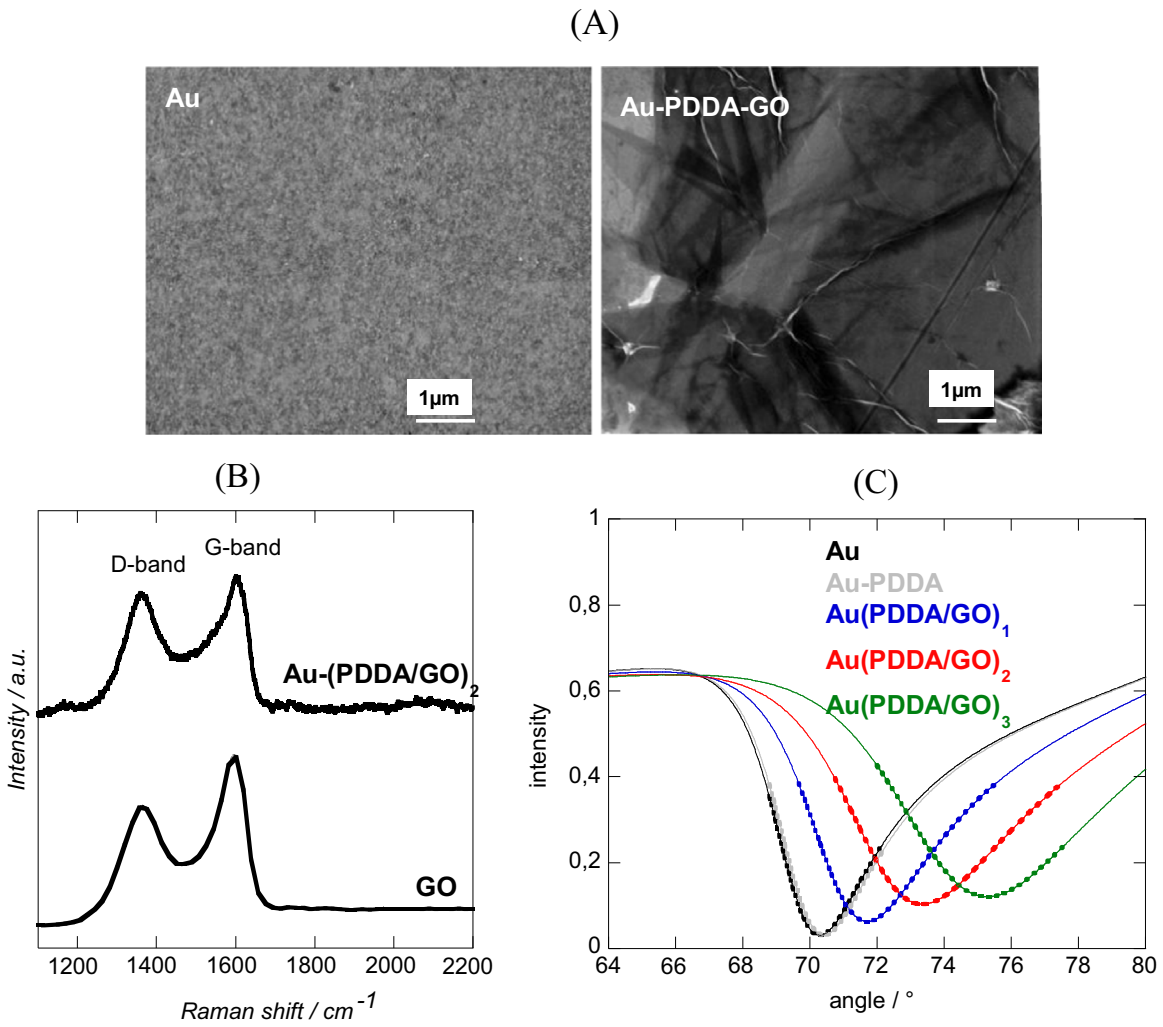

Fig. 2. (A) SEM image of gold (left) and gold modified with 2 layers of PDDA/GO; (B) Raman spectra of Au-$(PDDA/GO)_2$; (C) Angle-resolved SPR curves for different interfaces: Au (black), Au-PDDA (grey) Au-$(PDDA/GO)_1$ (blue), Au-$(PDDA/GO)_2$ (red) and Au-$(PDDA/GO)_3$ (green). The dotted lines are the experimental data and the solid lines are SPR fits [λ=670 nm, n_{prism}=1.52, n_{Ti}=2.36+i3.47 (d=5 nm), n_{gold}=0.197+i3.67 (d=50 nm), n_{PDDA}=1.55 (d=0.5 nm), $n_{dielectric}$=1.333; n_{GO}=2.75+i0.41]. (For interpretation of the references to color in this figure legend, the reader is referred to the web version of this article.)

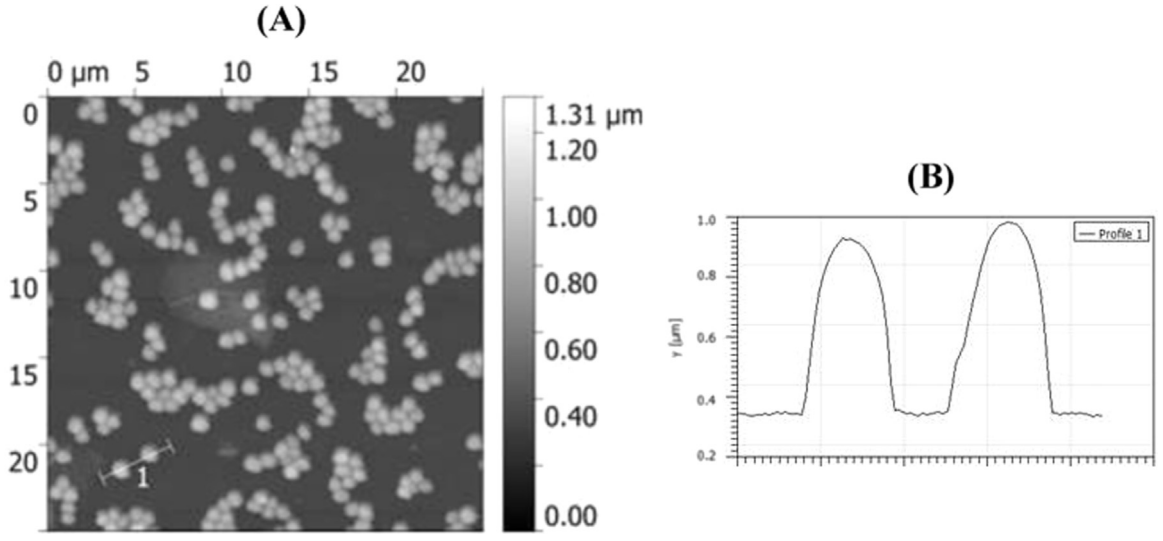

Fig. 3. (A) AFM image and (B) line profile of a Au-$(PDDA/GO)_2$ interface modified with *M. lysodeiktikus.*

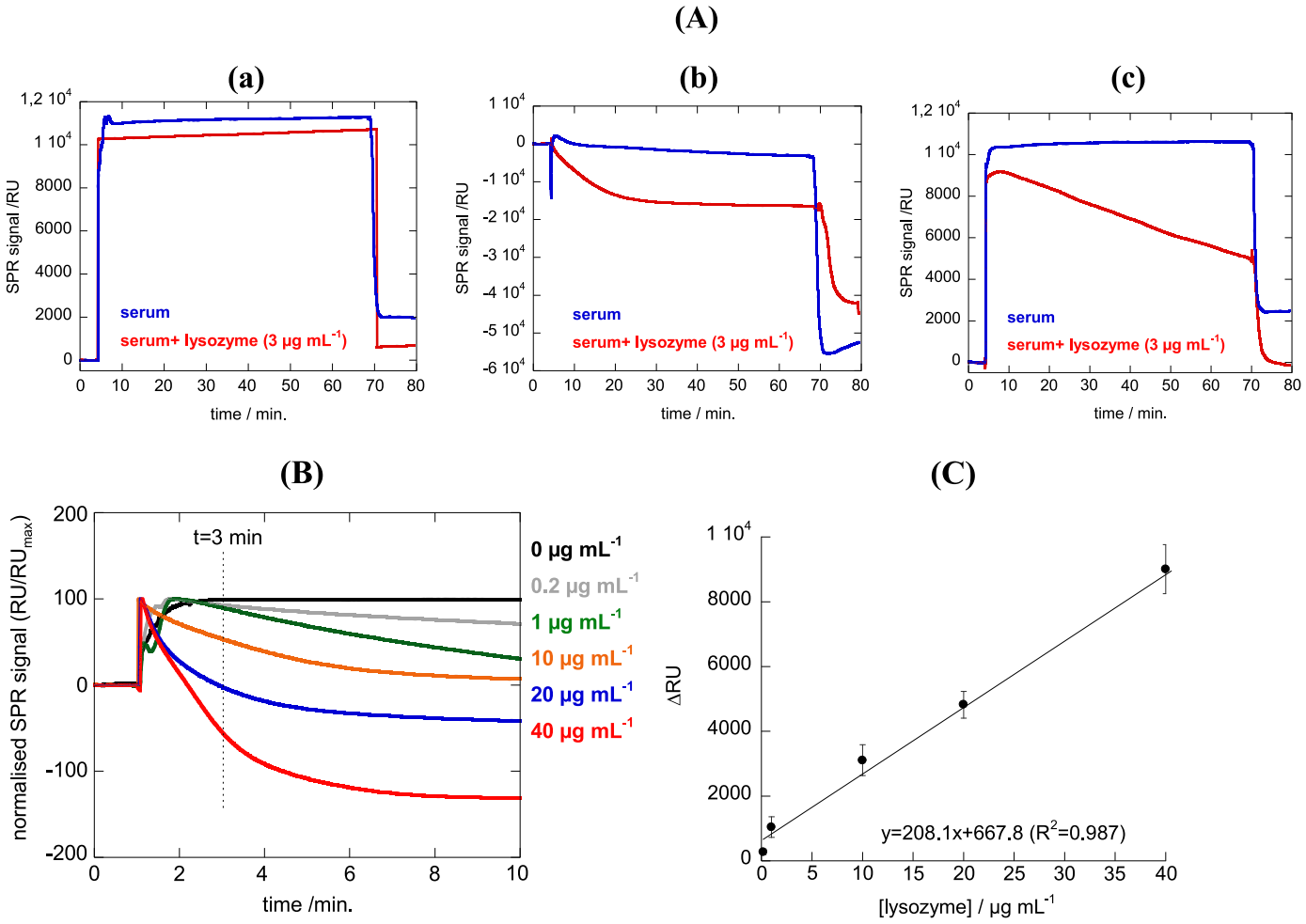

Fig. 4. (A) Sensograms upon the addition of serum (channel 1, blue) and serum spiked with lysozyme (3 µg mL^{-1}) (channel 2, red) using different SPR chips: (a) *M. lysodeikticus* directly adsorbed on Au; (b) *M. lysodeiktikus* adsorbed on Au-PDDA, (c) *M. lysodeikticus* modified Au-$(PDDA/GO)_2$ chips; (B) SPR response to different concentrations of lysozyme added to fetal bovine serum; (C) Calibration curve obtained by plotting the change in SPR signal after 3 min versus lysozyme concentration in the sample. (For interpretation of the references to color in this figure legend, the reader is referred to the web version of this article.)

assess the effect of serum on the biosensor, while the second one was used to investigate the same serum spiked with relevant concentrations of lysozyme. We first examined the interaction of *M. lysodeikticus* on gold and Au-$(PDDA/GO)_2$ SPR interfaces. Adsorption of bacteria on Au was not significant, resulting in a neglectable SPR change upon lysozyme addition (Fig. 4Aa). High levels of bacteria could be adsorbed *via* electrostatic interactions between the positively charged PDDA layer and the negatively charged bacterial membrane. This resulted in a more pronounced SPR decrease upon the addition of serum spiked with lysozyme than was the case for gold (Fig. 4Ab). However, the obtained PDDA/*M. lysodeikticus* sensors were not stable over time in water or serum. Addition of serum alone also resulted in a decrease of the SPR signal. Comparatively, when bacteria were adsorbed on Au-$(PDDA/GO)_2$, the stability issue was overcome (Fig. 4Ac): a decrease in SPR signal due to desorption of bacteria occurred only in the presence of lysozyme. Taken together this data allowed to conclude that GO assures a stable immobilization of whole bacterial cells of *M. lysodeikticus* on the sensor surface.

To limit non-specific adsorption of serum proteins to GO, the *M. lysodeikticus* modified Au-$(PDDA/GO)_2$ interface was in the following step blocked by immersion into BSA (3%) for 1 h. As seen in Fig. 4**B**, addition of serum resulted only in a small increase of the SPR signal over time. In contrast, serum spiked with different concentrations of lysozyme shows a significant decrease of the SPR signal over time, whose rate depends on the lysozyme concentration (Fig. 4**B**). The decrease of the SPR signal after 3 min scaled linearly with the concentration of lysozyme in the serum in the range from 0.2 to 40 µg mL^{-1} (Fig. 4**C**). Typical lysozyme levels in serum of healthy individuals are ≈ 1.7 µg mL^{-1} (Prockop and Davidson, 1964). People with renal diseases, leukemia or inflammatory gastrointestinal diseases show on the other hand lysozyme concentrations higher than 20 µg mL^{-1} and could even reach 100 µg mL^{-1} (Prockop and Davidson, 1964, Osserman and Lawlor, 1966, Perillie et al., 1968, Rubio, 2014). A limit of detection of 0.05 µg mL^{-1} (3.5 nmol L^{-1}) was calculated based on 3 × standard deviation for the response of biosensor to blank serum, without lysozyme. These analytical characteristics compare well with those reported for other lysozyme sensors in serum or real samples (Table 1). The reproducibility and storage stability of the sensor were determined by analyzing a sample of serum spiked with 1 µg mL^{-1} lysozyme. The RSD of the SPR response of 3 different sensors was 14%. After 1 week of storage at 2–8 °C in the fridge, the biosensor displayed 98% of the analytical signal recorded immediately after fabrication.

In addition, the whole cell biosensor provides a fast response of ≈ 3 min, without the need for signal amplification. Indeed, ELISA-based methods require several steps and a total analysis time of 4 h. While other sensing formats provide better sensitivity (Table 1), they are much more complex and require skilled users. The simple fabrication procedure makes this sensor a promising alternative.

Table 1
Analytical characteristics of different lysozyme sensors formats.

Ligand	Detection method	Sensing material or method details	Limit of detection	Reference
Aptamer	SPR	rGO on Au	5×10^{-10} mol L^{-1}	(Subramanian et al., 2013)
Aptamer	SPR	Thiol on Au	2.4×10^{-9} mol L^{-1}	(Mihai et al., 2015)
MIP	SPR	PEDMAH nanoparticles attached on Au	3.2×10^{-8} mol L^{-1}	(Sener et al., 2011)
Aptamer/ antibody	DPV	SPCE	4.3×10^{-15} mol L^{-1}	(Ocana et al., 2015)
Antibody	ELISA/Spectro-photometric	Antibody coated polystyrene ELISA wells	5.4×10^{-11} mol L^{-1}	Human Lysozyme EIA kit
Aptamer	SERS	Aptamer-based +gold nanoparticles	1×10^{-15} mol L^{-1}	(He et al., 2013)
MIP	QCM	MIP on Au	8.4×10^{-11} mol L^{-1}	(Sener et al., 2011)
Aptamer	Fluorescence	"Feed-Forward" Network of DNA-Related Reaction Cycles	2.0×10^{-14} mol L^{-1}	(Ren et al., 2012)
Micrococcus lysodeikticus	SPR	Whole bacterial cells adsorbed on PDDA-GO coated Au	3.5×10^{-9} mol L^{-1}	This work

rGO (reduced graphene oxide); PEDMAH (Poly(ethylene glycol dimethacrylate-*N*-methacryloyl-L-histidine methylester); SPCE: screen-printed carbon electrode. PRLS: Plasmon Resonance, DPV:differential pulde volammetry. MIP: molecularly imprinted polymer. Light Scattering. QCM: Quartz Crystal Microbalance, SERS: Surface enhanced Raman scattering.

The specificity of the sensor was investigated with fetal bovine serum spiked either with human Ig G (10 mg/mL), trypsin (400 μg/L) or a mixture of penicillin and streptomycin (20 μg/mL). The average signals for n=3 sensors were well below the detection limit, being 196, 61 and −236 RU, respectively, where the negative signal for antibiotics denotes an increase in reflectivity during the 3 min analysis. The effects of serum constituents at their typical concentrations (Stoop et al., 1969, Line et al., 1970, Buamah and Skillen, 1985) is negligible in comparison with desorption of *M. lysodeikticus* cells due to fast kinetics of lysozyme's enzymatic reaction. The whole cell bacterial biosensor presented here is adequate for lysozyme detection in undiluted serum as a useful indicator in leukemia, renal diseases and inflammatory gastrointestinal diseases.

3.3. Mechanistic considerations

The presence of lysozyme in serum impacts in two different ways the SPR signal. It removes a significant part of the adsorbed bacteria (see Fig. 3 in comparison with Fig. 5**A**). Indeed, *M. lysodeikticus* modified surfaces carried 387,000 ± 26000 bacteria per

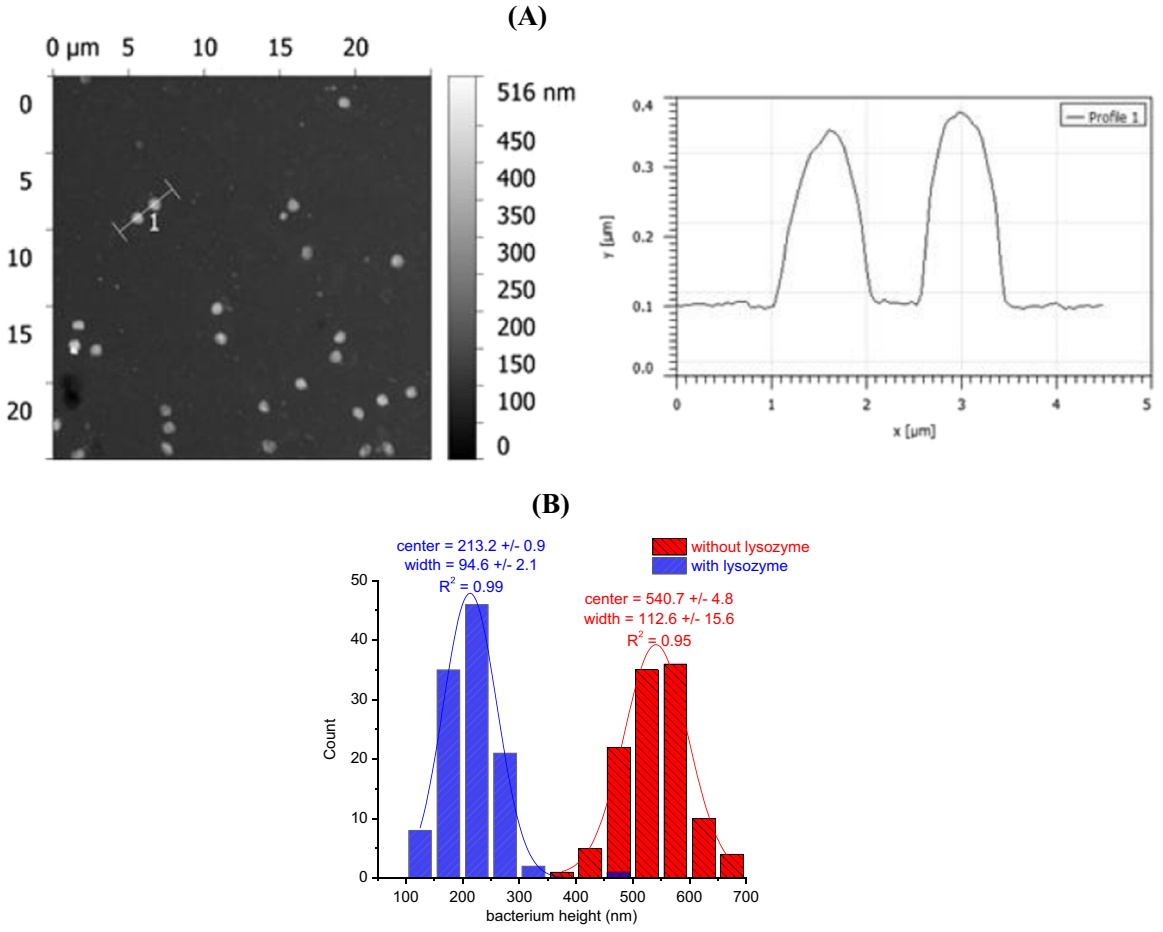

Fig. 5. (A) Representative AFM image and line profile of a *M. lysodeikticus* modified Au-$(PDDA/GO)_2$ chip after exposure to serum spiked with lysozyme (10 μg mL^{-1} for 1 h); (B) Height distributions of the surface-immobilized bacteria before (red) and after (blue) exposure to lysozyme 10 μg mL^{-1} for 1 h). (For interpretation of the references to colors in this figure legend, the reader is referred to the web version of this article.)

1 mm^2 before exposure to lysozyme and 46,000 ± 4200 bacteria per 1 mm^2 after exposure to lysozyme (10 μg mL^{-1} in serum for 60 min). The decrease in the SPR signal in the presence of lysozyme is thus mostly linked to the desorption of *M. lysodeikticus* bacterial cells (Fig. 1).

In addition, a change in the height of *M. lysodeikticus* takes place. From analysis of the height of surface-adsorbed *M. lysodeikticus,* before and after exposure to lysozyme in serum (Fig. 5**B**), the average height of 537 ± 56 nm decreased to 215 ± 50 nm after lysozyme (10 μg mL^{-1}) exposure. Lysozyme is thus clearly causing the "shrinkage" of *M. lysodeikticus*. Taking into account the penetration depth of the surface plasmons, which is around hundreds of nm, this "shrinkage" also contributes to the decrease of the signal of our sensor. To conclude, lysozyme does not simply replace the *M. lysodeikticus* cells as one can expect considering the high affinity of lysozyme for GO (Li et al., 2014). Lysozyme binding affects cell wall integrity, causing the cell clusters to break apart in the first instance, followed by cell detachment.

4. Conclusions

The suitability of *M. lysodeikticus*-modified, GO-coated SPR interfaces to sense lysozyme in serum is demonstrated. GO was integrated onto gold interfaces using layer-by-layer deposition of polycationic polymer PDDA and GO. Absorption of whole cells of *M. lysodeikticus* onto GO and blocking remaining GO sites with BSA (3%) formed a reproducible non-fouling surface for the sensing of lysozyme in serum samples. The detection mechanism is based on the sensitive monitoring of lysozyme concentration-dependent desorption of *M. lysodeiktikus* cells from the sensor surface. This desorption, together with a significant change in morphology of the bacterial cell, causes a characteristic decrease of the SPR signal. The sensor has a wide dynamic range, with a limit of detection of 0.05 μg mL^{-1}. This detection limit, achieved in undiluted serum, recommends our sensor for clinical use.

Acknowledgements

Financial support from Marie Curie International Reintegration Grant FP7 PEOPLE-2010-RG-277126 for A.V. is gratefully acknowledged. S.G., M.G., S.D. and V.D. thank the Romanian Executive Unit for Higher Education, Research, Development and Innovation Funding for funding through grants PN II-ID-PCCE-2011-2-0075 (for S.G., M.G. and S.D.) and PN II-RU-TE-2014-4-2434 (for V.D.). R.B. and S.S. gratefully acknowledge financial support from the Centre National de la Recherche Scientifique (CNRS), the University Lille 1 and the Nord Pas de Calais region. S.S. thanks the Institut Universitaire de France (IUF) for financial support. Q.W. thanks "the Fundamental Research Funds of Shandong University", under Grant no. 31370074614039.

Appendix A. Supporting information

Supplementary data associated with this article can be found in the online version at http://dx.doi.org/10.1016/j.bios.2016.03.040.

References

Abdulhalim, I., Zourob, M., Lakhtakia, A., 2008. J. Electromagn. 28, 213–242.
Avanti, C., Saluja, V., van Streun, E.L.P., Frijlink, H.W., Hinrichs, W.L.J., 2014. PLoS One 9, e86244.
Buamah, P.K., Skillen, A.W., 1985. Clin. Chem. 31, 876–877.
Cheng, A.K.H., Ge, B., Yu, H.-Z., 2007. Anal. Chem. 79, 5158–5164.
Chiu, N.F., Huang, T.Y., 2014. Sens. Actuators B 197, 35–42.
Chung, K., Lee, J.E., Kim, J.E., Kim, Y., Yang, H., Kim, S.O., Kim, D., Kim, D.H., 2015. ACS Appl. Mater. Interfaces 7, 144–151.
He, P., Zhang, Y., Liu, L., Qiao, W., Zhang, S., 2013. Chem. Eur. J. 19, 7452–7460.
Huang, C.F., Yao, G.H., Liang, R.P., Qiu, J.D., 2013. Biosens. Bioelectron. 50, 305–310.
Hun, X., Chen, H., Wang, W., 2010. Biosens. Bioelectron. 26, 248–254.
Li, L.-D., Chen, Z.-B., Zhao, H.-Z., Guo, L., Mu, X., 2010. Sens. Actuators B 149, 110–115.
Li, S., Mulloor, J.J., Wang, L., Ji, Y., Mulloor, C.J., Micic, M., Orbulescu, J., Leblanc, M., 2014. ACS Appl. Mater. Interfaces 6, 5704–5712.
Line, D.H., Poole, G.W., Waterworth, P.M., 1970. Tubercle 51, 76–81.
Ma, J., Cai, P., Qi, W., Kong, D., Wang, H., 2013. Coll. Surf. A 426, 6–11.
Mao, Y., Bao, Y., Wang, W., Li, Z., Li, F., Niu, L., 2011. Talanta 85, 2016–2112.
Matsunaga, T., Hishiya, T., Takeuchi, T., 2007. Anal. Chim. Acta 591, 63–67.
Mihai, L., Vezeanu, A., Polonschii, C., Albu, C., Radu, G.L., Vasilescu, A., 2015. Sens. Actuators B 206, 198–204.
Ocana, C., Hayat, A., Mishra, R.K., Vasilescu, A., Del Valle, M., Marty, J.-L., 2015. Bioelectrochemistry 105, 72–77.
Osserman, L.F., Lawlor, D.P., 1966. J. Exp. Med. 124, 921–952.
Perillie, P.E., Kaplan, S.E., Lejkowitz, E., Rogaway, W., Finch, S.C., 1968. JAMA 203, 317–322.
Prockop, D.J., Davidson, W.D., 1964. N. Engl. J. Med. 270, 270–274.
Ren, R., Yu, Z., Zou, Y., Zhang, S., 2012. Chem. Eur. J. 18, 14201–14209.
Rubio, C.A., 2014. Pathogens 3, 73–92.
Sener, G., Uzun, L., Say, R., Denizli, A., 2011. Sens. Actuators B 160, 791–799.
Shalabney, A., Abdulhalim, I., 2011. Laser Photon. Rev. 5, 571–606.
Singh, M., Holzinger, M., Tabrizian, M., Winters, S., Berner, N.C., Cosnier, S., Duesberg, G.S., 2015. J. Am. Chem. Soc. 137, 2800–2803.
Stoop, J.W., Zegers, B.J., Sander, P.C., Ballieux, R.E., 1969. Clin. Exp. Immunol. 4, 101–112.
Subramanian, P., Barka-Bouaifel, F., Bouckaert, J., Yamakawa, N., Boukherroub, R., Szunerits, S., 2014. ACS Appl. Mater. Interfaces 6, 5422–5431.
Subramanian, P., Lesniewski, A., Kaminska, I., Vlandas, A., Vasilescu, A., Niedziolka-Jonsson, J., Pichonat, E., Happy, H., Boukherroub, R., Szunerits, S., 2013. Biosens. Bioelectron. 50, 239–243.
Szunerits, S., Castel, X., Boukherroub, R., 2008. J. Phys. Chem. C 112, 10883.
Szunerits, S., Maalouli, N., Wijaya, E., Vilcot, J.-P., Boukherroub, R., 2013. Anal. Bioanal. Chem. 405, 1435–1443.
Szunerits, S., Shalabney, A., Boukherroub, R., Abdulhalim, I., 2012. Rev. Anal. Chem. 31, 15–28.
Touahir, L., Jenkins, A.T.A., Boukherroub, R., Gouget-Laemmel, A.C., Chazalviel, J.-N., Peretti, J., Ozanam, F., Szunerits., S., 2010. J. Phys. Chem. C 114, 22582.
Wang, L., Zhu, C., Han, L., L., J., Zhou, M., Dong, S., 2011. Chem. Commun. 47, 7794–7796.
Zagorodko, O., Bouckaert, J., Dumych, T., Bilyy, R., Larroulet, I., Yanguas Serrano, A., Dorta, D.A., Gouin, S.G., Dima, S.-O., Oancea, F., Boukherroub, R., Szunerits, S., 2015. Biosensors 5, 276–287.
Zagorodko, O., Spadavecchia, J., Yanguas Serrano, A., Larroulet, I., Pesquera, A., Zurutuza, A., Boukherroub, R., Szunerits, S., 2014. Anal. Chem. 86, 11211–11216.
Zhang, H., Sun, Y., Gao, S., Zhang, J., Zhang, H.Q., Song, D.Q., 2013a. Small 9, 2537–2540.
Zhang, H., Sun, Y., Wu, Q., Zhang, H., Bai, Y., Song, D.Q., 2013a. Analyst 138, 7175–7181.
Zhang, H., Sun, Y., Xu, B., Zhang, J., GAO, Y., Zhang, H.Q., Song, D.Q., 2013b. Biosens. Bioelectron. 45, 230–236.